Bulletin of the Seismological Society of America. Vol. 67, No. 3, pp. 693-711. Juue 1977

THE APRIL 29, 1965, PUGET SOUND EARTHQUAKE AND THE CRUSTAL AND UPPER MANTLE STRUCTURE OF WESTERN WASHINGTON

By Charles A. Langston and David E. Blum

ABSTRACT

Simultaneous modeling of source parameters and local layered earth structure for the April 29, 1965, Puget Sound earthquake was done using both ray and layer matrix formulations for point dislocations imbedded in layered media. The source parameters obtained are: dip 70° to the east, strike 344°, rake −75°, 63 km depth, average moment of $1.4 \pm 0.6 \times 10^{26}$ dyne-cm, and a triangular time function with a rise time of 0.5 sec and falloff of 2.5 sec. An upper mantle and crustal model for southern Puget Sound was determined from inferred reflections from interfaces above the source. The main features of the model include a distinct 15-km-thick low-velocity zone with a 2.5-km/sec *P*-wave-velocity contrast lower boundary situated at approximately 56-km depth. Ray calculations which allow for sources in dipping structure indicate that the inferred high contrast value can trade off significantly with interface dip provided the structure dips eastward. The effective crustal model is less than 15 km thick with a substantial sediment section near the surface. A stacking technique using the instantaneous amplitude of the analytic signal is developed for interpreting short-period teleseismic observations. The inferred reflection from the base of the low-velocity zone is recovered from short-period *P* and *S* waves. An apparent attenuation is also observed for *pP* from comparisons between the short- and long-period data sets. This correlates with the local surface structure of Puget Sound and yields an effective Q of approximately 65 for the crust and upper mantle.

Introduction

A previous paper dealt with the problem of trying to deduce source parameters from an extremely shallow earthquake, the Koyna event of December, 1967 (Langston, 1976a). The interference of the direct waves and surface reflections was very severe due to the depth of the Koyna hypocenter. Some speculations were made to the origin of some of the reverberations after the reflections but these were hampered by both ignorance of the Koyna crustal structure and the interference with the major phases. If, however, an earthquake is deep enough so that the surface reflections and the direct wave are well separated, perhaps layer interfaces between the hypocenter and free surface can be resolved by intermediate reflected arrivals. It is exactly this supposition which will be used to explain the shape of long-period P waves from the Puget Sound earthquake. A crust model for southern Puget Sound will be deduced by identifying arrivals between P and pP as underside reflections from crustal layers. A major compressional and shear-wave low-velocity zone (LVZ) in the uppermost mantle will be proposed by modeling the time, amplitude, and polarity of these reflected arrivals. Simultaneously, care will be taken to model the source parameters as well.

Geologic and Tectonic Setting

Puget Sound is located in northwestern Washington and is part of a major north-south geologic and physiographic province, the Puget-Willamette depression (Figure

1) (Snavely and Wagner, 1963). The geologic development of this area has been controlled by Tertiary sedimentation and volcanism in a north-south trending eugeosyncline shown in Figure 1 (Snavely and Wagner, 1963; Snavely *et al.*, 1968). The Puget-Willamette depression may be fault controlled with major faults occurring on the eastern margin of Puget Sound and the western side of the Willamette Valley (Algermissen and Harding, 1965; Bromery and Snavely, 1964).

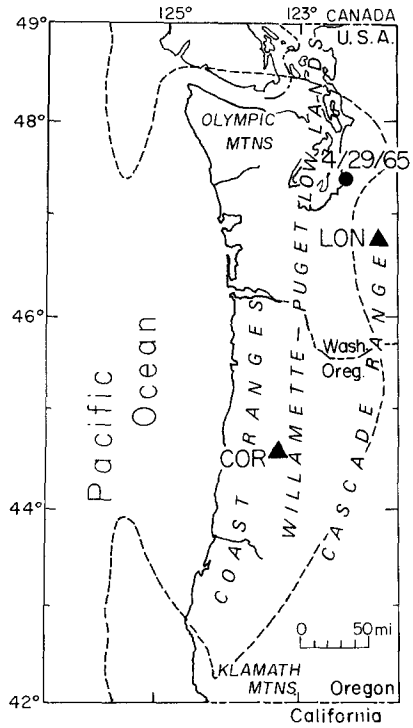

FIG. 1. Index map of western Washington and Oregon showing the epicenter of the 1965 Puget Sound event and WWSSN stations used in the receiver structure determination. The dashed line is the approximate extent of the Tertiary eugeosyncline, after Snavely and Wagner (1963).

Land seismic refraction measurements are relatively sparse for the general area with several unreversed profiles composing the data set. The work of Berg *et al.* (1966), Tatel and Tuve (1955), and Zuercher (1975) suggest that the crust of the Oregon Coast Ranges, Olympics, and southern Puget Sound is thin, being on the order of 16 to 20 km. Because of the conspicuous lack of pre-Tertiary granitic basement within the margins of the Tertiary eugeosyncline (Figure 1) and from the velocity and thickness values obtained from some of these refraction profiles, some authors have suggested that the area is a large embayment of oceanic crust in the North American Continent (Hamilton and Myers, 1966; Dickinson, 1970). However, northward at Vancouver Island, White and Savage (1965) obtained a crustal thickness in excess of 50 km. The studies by Zuercher (1975) and Crosson (1976) also suggest that central Puget Sound may be a local crustal depression in which the moho occurs at greater than 30 km depth.

Through detailed gravity and magnetic modeling, Daneš *et al.* (1965) deduced some of the major structures of southern Puget Sound. Their principal results include the discovery of a large northwest trending igneous horst structure with flanking deep sedimentary basins. They infer sediment thicknesses of 4 and 10 km for the southern Tacoma basin and northern Seattle basin, respectively. The large observed gravity gradients suggest major faults bounding this horst with inferred throws on the order of several kilometers. It may be significant that the April 1965 event occurred under the eastern edge of this structure. Daneš (1969) has also suggested that Puget Sound is a great isostatic depression with an isostatic anomaly greater than −100 mgal.

The comparison of these geophysical studies suggests that Puget Sound is an extremely complex area of tectonic downwarping with the possibility of high gradients on crustal layer interfaces and with complicated subsurface geology. On a regional scale it may represent the transition between the Coast Range-Olympic province to the west with the Cascades to the east and Canadian Insular belt to the north.

The theory of plate tectonics forms the basis for current thinking on the tectonic framework of the Pacific Northwest. Interpretation of the magnetic anomalies of Raff and Mason (1961) by Vine and Wilson (1965), Wilson (1965), and Vine (1966) and other subsequent work by Tobin and Sykes (1968), Atwater (1970), Dickinson (1970), Silver (1971a, 1971b, 1972), Crosson (1972), and Chandra (1974), among others, have led to a hypothesis relating the geophysical and geologic data into one plate tectonic scheme. The model states that subduction of oceanic crust and upper mantle is taking place north of Cape Mendocino to Vancouver Island. A small offshore ridge system, the Gorda-Juan de Fuca rise, is still producing oceanic lithosphere which is the remnant of the previously more extensive Farallon plate (Atwater, 1970). Spreading at a half-rate of about 2.5 cm/year, this small plate may still be underthrusting the continent as the association of andesitic vulcanism in the Cascades seems to require (Dickinson, 1970) and as inferred from offshore geologic evidence (Silver, 1971a, 1972). Against the normal assumptions of plate tectonics, this small plate does not appear to be rigid, but seems to be experiencing internal deformation (Silver, 1971b; Crosson, 1972).

Perhaps the most serious problem with this scheme is the conspicuous absence of a seismic Benioff zone. The general seismicity level of the area is low other than at the offshore fracture zones (Tobin and Sykes, 1968; Chandra, 1974). Puget Sound has a moderate background of diffuse seismicity, however, and a few events have occurred at depths of up to 70 km (Crosson, 1972). The magnitude 6.5 Puget Sound earthquake of April 1965 was located at 60 km depth, see Figure 1 (Algermissen and Harding, 1965), and the somewhat larger April 1949 event, at 70 km (Nuttli, 1952). Although these events are not extremely deep for other island and continental arcs, they are very unusual compared to all other continental U.S. earthquakes. Because of this, they have been cited as evidence for a remnant of a subducting plate, or perhaps, a very slowly subducting plate under Washington (Isacks and Molnar, 1971; Crosson, 1972). Other geophysical evidence supporting this plate model comes from travel-time anomalies determined from P residuals for the 1965 event (McKenzie and Julian, 1971) and from an array-processing study using teleseismic P arrivals at Puget Sound (Lin, 1974). Both of these studies reach the similar conclusion that a high wave-velocity plate dips to the east with an angle of about 50°.

The unusual depth of the April 1965 event and the interesting geologic and geophysical problems this area presents motivates the detailed wave-form study that

this paper reports. The original purpose of this study was to find a detailed source model for the earthquake, but as it turned out, much more interesting information could be found by modeling the local source structure as well.

The Puget Sound Earthquake

On April 29, 1965, at 15:28:44 GMT a magnitude 6.5 earthquake shook the environs of southern Puget Sound causing moderate damage in Seattle and Tacoma. The location of the epicenter was midway between these two cities and the hypocentral depth estimated to be at 60 km (Algermissen and Harding, 1965). Consistent focal mechanisms for the event done by several authors show predominantly normal dip-slip movement on a 70° eastward dipping plane striking approximately 15° west of north (Algermissen and Harding, 1965; Isacks and Molnar, 1971; Chandra, 1974). The auxiliary plane is only poorly constrained because of sparse local station coverage, a common occurrence for this type of orientation. Because of excellent teleseismic coverage, however, the first nodal plane is extremely well determined and serves as a very useful constraint in the wave-form modeling.

Data and Data Processing

The gathering and processing of long-period *P*- and *SH*-wave forms were done as described in Langston (1976a). Table 1 lists the WWSSN stations utilized for this study. Unfortunately, there was only one station in which the horizontal components were naturally rotated with respect to the ray direction. As a result, only a few *SH*-wave forms could be salvaged for wave-shape analysis and even these may be contaminated by the rotation process.

Most of the stations in Table 1 were equipped with the longer-period 30–100 instrument instead of the 15–100 instrument used in the Koyna study. A few stations, ANT, QUI, SJG, and BEC had just been changed to the standard 15–100 instrument, however, so these were equalized to be consistent with the rest of the data set. An operator was constructed and convolved with these data to effectively make them 30–100 observations. The 30–100 instrument response was calculated using Hagiwara's (1958) formulation.

Data Inversion and Interpretation

As a starting point, it would be most convenient to present the final inferred earth and source models and *P*-wave-form fits. The complex interactions of the earth and source models will then be examined point by point and the reasoning behind each effect presented in a coherent manner.

Figure 2 displays the results of trial and error wave-form modeling to find a source and earth model most consistent with the long-period data. A standard first-motion plot (*bottom hemisphere*) is given in the center of the diagram with the *P* nodal planes inferred from this study. In this determination, *pP* as well as *P* first motions were incorporated. Lines are drawn from each observed synthetic wave-form pair to the appropriate spot on the focal sphere which represents the downgoing *P* ray at that station. For each seismogram pair the observed is plotted above the synthetic. The source orientation parameters are given in the corner of Figure 2. In this model the source is assumed to be a single point dislocation with a triangular time function characterized by a rise and falloff time δt_1 and δt_2 equal to 0.5 and 2.5 sec, respectively. The final plane-layered earth model is presented in Figure 3 and is under the

TABLE 1

STATION INFORMATION

Station	Δ (deg.)	Azimuth (deg.)	BAZ (deg.)	Components*
AFI	75.3	229.7	32.3	*P*, *p*(d)
AKU	53.2	30.1	304.7	*p*(b)
ANP	87.8	305.5	37.6	*P*
ANT	84.8	133.6	327.5	*P*, *p*(d)
ARE	78.2	130.5	327.5	*s*
ATL	31.8	102.2	307.4	*P*, *p*(a)
ATU	89.8	26.2	337.7	*P*, *p*(d)
BEC	45.7	87.6	306.7	*P*, *p*(b)
CAR	59.2	109.5	319.4	*P*, *p*(b), *s*
COP	70.5	25.3	329.2	*P*, *S*
ESK	65.6	33.3	319.3	*p*(c)
GDH	39.4	31.6	272.9	*P*, *p*(a), *S*
GEO	33.7	87.8	299.5	*P*, *p*(a)
GIE	55.5	140.0	334.1	*p*(b)
GUA	82.0	281.2	43.3	*P*
HNR	88.7	254.7	41.6	*P*, *p*(d)
IST	88.3	21.3	340.9	*P*, *p*(d)
KEV	61.0	11.7	336.6	*P*, *p*(c)
KON	66.3	24.4	326.5	*P*
KTG	49.5	25.9	298.4	*P*, *p*(b), *S*
LPB	80.0	127.8	326.0	*P*, *p*(d), *s*
MAL	79.5	46.2	322.4	*P*
NNA	71.7	132.7	329.3	*P*, *S*
NOR	45.7	11.4	293.8	*s*
NUR	69.2	16.8	336.6	*P*, *p*(c), *s*
OGD	34.3	82.8	297.0	*p*(a)
PDA	67.4	58.6	313.0	*P*
PTO	74.1	46.0	319.7	*P*, *p*(c), *S*
QUI	60.8	127.5	327.4	*P*
SCP	32.2	85.2	296.9	*P*
SHA	31.0	110.2	312.3	*P*
SJG	54.1	102.8	315.8	*P*
STU	75.4	30.8	328.3	*P*, *p*(d)
TOL	77.2	44.0	322.1	*P*, *s*
TRN	62.6	104.7	318.1	*P*, *p*(c)
UME	65.3	17.3	332.9	*p*(c), *s*
VAL	65.3	39.2	316.1	*p*(c), *S*
WES	35.9	78.8	295.9	*P*, *p*(a)

*P, long-period vertical *P*-wave form or first motion. *p*(a), short-period vertical *P*-wave form. Letter in parenthesis designates stacking group. *S*, long-period tangential *S*-wave form. *s*, short-period horizontal *S*-wave forms used in stacking.

heading of "PS-9" in Table 2. The source is situated at a depth of 63 km for this model.

Both ray theory (Langston and Helmberger, 1975) and propagator matrix techniques (Haskell, 1953; Harkrider, 1964; Fuchs, 1966) were used to calculate synthetic seismograms for a point dislocation in a layered elastic medium. Both methods are equivalent and complementary for various model calculations. Ray theory has the advantage of giving a direct physical interpretation to observed phases. Matrix

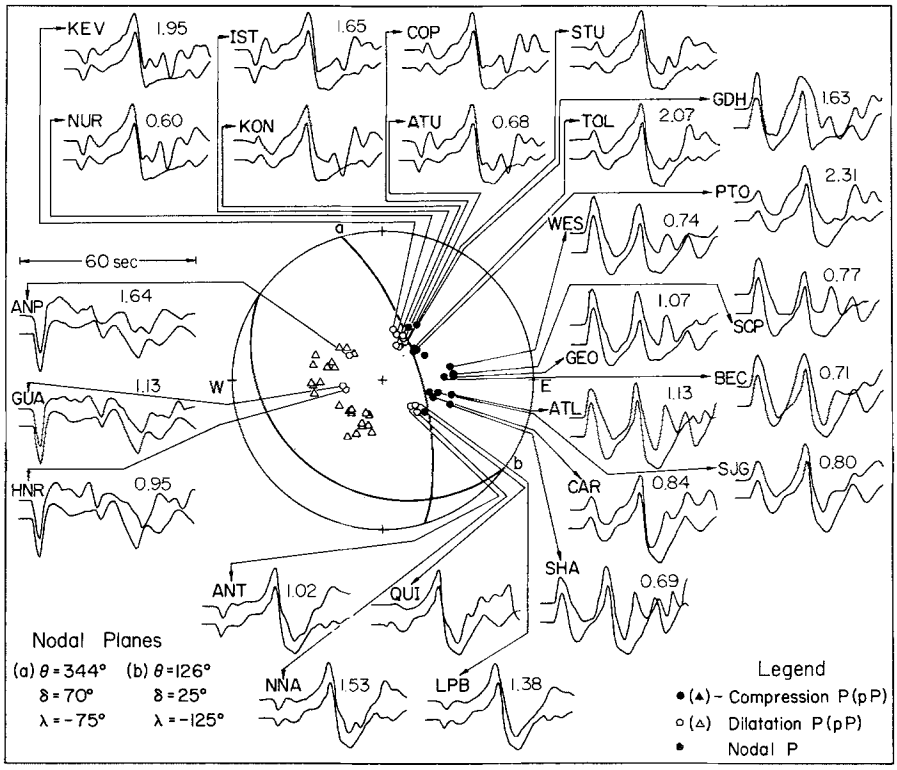

FIG. 2. Comparison of synthetic and observed P-wave forms for the final source and earth structure models. The observed is displayed directly above the synthetic at each station with the calculated moment indicated next to the traces ($\times 10^{26}$ dyne-cm). The focal plot is for the bottom hemisphere.

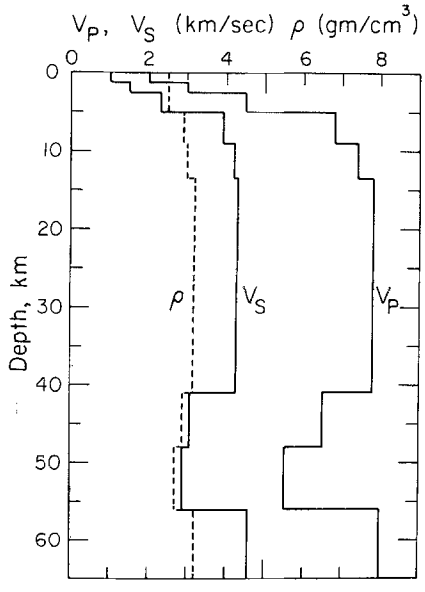

FIG. 3. PS-9 earth model for Puget Sound.

techniques, while exact in terms of including all multiples, give little insight into the model but do serve as a check to the ray calculations. It can also be used as a tool for calculating the effect of gradients in the earth model by approximating them with many thin layers.

Two striking features are apparent in Figures 2 and 3. The first is the quality of the wave-form fits over the entire azimuth range. The observed wave forms have a tremendous variation in shape as a function of azimuth and take-off angle which the model approximates quite nicely for nearly all stations. Second, the earth model presented in Figure 3 is quite unusual. The major features of PS-9 include a very distinct and large low-velocity zone between 41 and 56 km depth. This structure is sandwiched between what appears to be mantle velocity material. The crustal section at the top is very thin, less than 15 km, and has very low-velocity materials near the free surface. This model was inferred entirely from the long-period P waves and will be discussed by closely examining which characteristics of the P waves control its various details.

Let us first look at what effects a simple earth model, a layer over a half-space, gives for the long-period P response. Figure 4 compares the simple one layer model (Table 2) with PS-9 for representative P-wave forms. The major phases P, pP, and sP are quickly apparent in these wave-form comparisons although there are significant differences in the interval between the direct P wave and pP. The small arrival several seconds before pP in the one-layer model is the P reflection from the bottom of the layer except at GUA where it is an S to P conversion at reflection. The first 18 sec

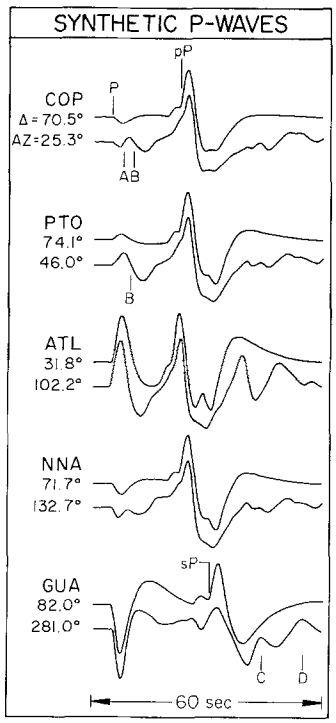

FIG. 4. Comparison of P-wave synthetic seismograms at five representative stations for the one-layer model (*top*) and PS-9 (*bottom*). The phase identifications are referred to in the text.

of the P wave for the simple model is just the convolution of the source time function with the Q operator and the instrument response since there are no distortions due to near-source structure.

For COP and stations like it in the northeast (see Figure 2), the first 18 sec of the observed P wave show at least two arrivals after the dilatational direct P. First there is an equal sized compression, arrival A (Figure 4) approximately 2 sec after P with another dilatational arrival, arrival B, 2 sec after that. Examination of the one-layer model of COP demonstrates that the overswing of the instrument response is not a factor here. At PTO the direct wave and arrival A have the same sign and add constructively because of the change in the P radiation pattern. This shows up as an increase in the P amplitude, relative to pP, at PTO and at other similar stations. Arrival B is plainly the same polarity as at COP. The interpretation of these arrivals is based on the assumption that they represent underside reflections from discontinuities above the source and not from source complications. It is entirely reasonable to assume that there are major discontinuities between a 60-km-deep source and the free surface, but it is obviously extremely hard to prove, unequivocally, that small arrivals are from such reflections and not source effects. The seismograms of Figure 2 suggest that these arrivals are associated with pP rather than the direct P wave by the observation that when direct P changes polarity, the A and B arrivals remain constant.

Assuming that these arrivals came from reflectors above the source, what can be said about their properties? Since the strength of upgoing P determines the amplitude of the reflection as well as the material contrasts, an approximate determination of the velocity contrast can immediately be made. At the northeastern P nodal stations upgoing SV radiation is at minimum because of fault orientation so that only P interactions can be considered. A cursory examination of the wave forms gives a minimum amplitude estimate for reflection A of about 0.15. This is clearly an underestimate since interference with the direct wave knocks it down considerably. There must be interference since the width of the first swing changes as a function of P amplitude and azimuth. Compare STU and TOL, Figure 2, for example. The type of contrast can immediately be deduced because of the known polarity of pP. Since upgoing P is dilatational and the reflection is compressional, the reflection coefficient must be negative, which implies a higher- to lower-velocity contrast. Simultaneously modeling the time function, relative timing, and relative amplitudes of direct P and phase A for the northeastern and southeastern stations yields the high contrast of 8.0 to 5.5 km/sec for the lowermost boundary of PS-9, Figure 3.

Continuing this line of reasoning one step further to phase B gives some remarkable results. Using the same process for finding the sign of the reflection coefficient, the polarity of B suggests that it comes from a lower- to higher-velocity contrast. Phase B, therefore, delimits the top of a low-velocity zone. Figure 5 demonstrates this explicitly for the station KEV. Ray number one is normalized to unity and all other ray amplitudes referenced to it. The top of the LVZ was modeled with two interfaces in order to increase the width of the reflected pulse. This particular model explains the azimuthal variation of wave shapes for the first 18 sec remarkably well (Figure 2).

The uncertainty in orientation (see Figure 2) is not a major factor in the modeling. The P first-motion data constrain the north-south nodal plane to within a degree. Since all of the stations are near the center of the plot and most are close to the nodal plane, relatively large variations in the rake ($-90 \pm 20°$) do little to affect the rela-

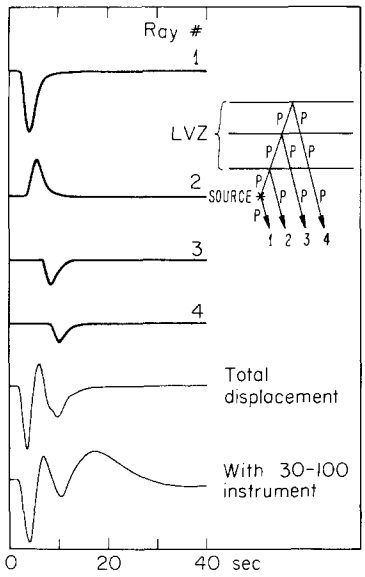

FIG. 5. KEV ray summation showing the effects caused by reflections from interfaces bounding the inferred LVZ.

tive amplitudes of P and pP. Upgoing SV is more sensitive so there is some basis for assigning the particular value used, although it is a small effect and will be discussed later. The velocity assigned to the source layer is a value typically found for these depths in upper mantle studies. Variations in this velocity, of up to ± 0.5 km/sec, don't significantly affect the results since we are looking at relative amplitudes and velocity contrasts only. This does point out that the absolute values of velocity for any part of the inferred model are somewhat ambiguous.

The phase pP and sP control and constrain the top of model PS-9. For the source function inferred from the direct P wave, it is evident that pP in a simple one-layer model (Figure 4) starts too sharply. The small arrival before pP suggests that a number of small reflections in the upper crust could give the desired effect of producing a smooth ramp before the main pP peak. Further evidence for this type of model occurs in the western stations HNR, GUA, and ANP. The predicted sP phase for the one-layer model is much too large and is not affected by small changes in the radiation pattern. The easiest way to cut down this amplitude is to lower the reflection coefficient by using low velocities near the top of the model. This implies many contrasts also, since there must be some kind of transition from mantle to sediment velocities. This is the basis for modeling the upper crust in model PS-9. It is interesting to note that the effective crustal section had to be kept thin since thicker crustal models caused spurious arrivals from the moho before the arrival time of pP. The absolute velocities for the top are not too well constrained. These values were determined by using the local refraction results of Berg *et al.* (1966) and Tatel and Tuve (1955). The lowest velocities are appropriate for Tertiary clastic rocks as reported in Press (1966). The mantle velocity above the LVZ of 7.8 km/sec was based on the data of Dehlinger *et al.* (1965), McCollum and Crosson (1975), and Zuercher (1975).

Note that we have approached the problem of assigning crustal velocities on the basis of inferred velocity contrast only. For example, Zuercher (1975) and Crosson (1976) have suggested from mine blast and earthquake travel-time data that mantle

velocities are only encountered at depths of 30 to 40 km in the central Puget Sound area. Linear gradients put in the models presented here to achieve this effect would have little expression in the resultant wave forms so long as average travel time was preserved. To keep computations simple, therefore, layers were kept as thick as warranted.

The S-wave velocity is one of the least constrained parameters in the model. The average S time is only constrained by sP, a phase which is distorted and reduced in size by the model. However, there is some evidence that large S-wave contrasts exist in the LVZ. At the western azimuth stations $S - P$ reflections were needed to reduce the backswing of the direct P (see GUA, Figure 4, for a comparison) and theoretical arrivals after sP were only obtained after increasing the shear-velocity contrast at the boundaries of the LVZ. These arrivals are shown as "C" and "D" in Figure 4 and are crustal multiples with substantial S to P conversions. Figure 2 shows that these multiples can help explain the arrivals after sP at these stations.

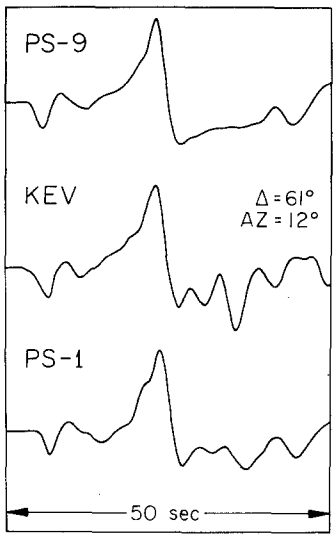

FIG. 6. Comparison of P-wave synthetic seismograms computed using the PS-1 and PS-9 earth models (Table 2) with the observation at KEV (*middle*).

These multiples bring up interesting questions concerning the arrivals after pP at the northeastern and eastern stations. PS-9 predicts a few crustal multiples after pP but nothing like those in some of the observations. Figure 6 shows the long-period P wave from the station KEV with a synthetic produced from the PS-9 model above and one made from a preliminary model, PS-1 (Table 2), below. The PS-1 model did not predict the LVZ interference effects very well nor the shape of pP for most observations. Because of the low shear velocities and higher contrasts this model has, compared to PS-9, crustal reverberations after pP are quite pronounced and fit the observations quite nicely for this azimuth. However, since it did not fit the front part of the record very well, in general, it was not used. This exercise demonstrates that the arrivals after pP could conceivably be explained by large velocity contrasts although lateral inhomogeneity would probably be needed to match them. These crustal and mantle reverberations sample larger portions of the model and at distances farther away from the epicenter as relative arrival times increase. Lateral changes over a

scale length of 50 km, not inconceivable for the region, coupled with the substantial depth of the source could be responsible for such effects. It must be mentioned that an added ambiguity inherent in this modeling is the lack of receiver characteristics. For the same reasons cited in the Koyna study (Langston, 1976a) no receiver responses were evaluated. Presumably, the effect for the vertical P wave is small but could be on the same order as the small arrivals behind pP. As such, these unknowns have to be considered a source of error in the study.

The evidence for constraining the rake angle of the north-south nodal plane comes from the relative amplitude of the reflection from the bottom of the LVZ. The observations of Figure 3.2 suggest that the reflection is more pronounced for the northern

TABLE 2
STRUCTURE MODELS

Layer No.	V_p (km/sec)	V_s (km/sec)	ρ (gm/cc)	Th (km)
		Model PS-1		
1	3.0	1.2	1.8	2.0
2	4.0	2.0	2.0	2.0
3	5.0	2.5	2.2	1.0
4	6.0	3.0	2.3	1.0
5	7.0	3.5	2.4	1.0
6	7.8	4.0	3.2	28.0
7	6.5	3.0	2.7	10.0
8	5.5	2.7	2.6	10.0
9	8.0	4.3	3.2	—
		Model PS-9		
1	2.0	1.0	2.5	1.2
2	3.0	1.5	2.5	1.2
3	4.5	2.3	2.5	2.5
4	6.8	3.9	2.9	4.0
5	7.4	4.2	3.0	4.5
6	7.8	4.3	3.2	27.3
7	6.5	3.1	2.9	7.0
8	5.5	2.9	2.7	8.0
9	8.0	4.6	3.2	—
		Model of Layer Over Half-space		
1	6.0	3.5	2.7	10.0
2	8.0	4.6	3.2	—

stations (KEV, NUR, etc.) compared to the southern stations (QUI, NNA, LPB, ANT). Rather than invoke extreme lateral heterogeneity for this interface, a simple explanation can be made for the effect using fault orientation. If the fault was pure dip-slip ($\lambda = -90°$), the northern and southern stations should be identical since the radiation pattern would be symmetric about a line perpendicular to the fault plane. Varying the rake angle strongly affects only the upgoing SV radiation since it is near a node for eastern azimuths and this type of orientation. It was found that the interference of S to P conversions with the P reflections decreased the amplitude of the LVZ phases where upgoing SV was comparatively large. Using this effect the rake angle was deduced to be approximately $-75°$ rather than pure dip-slip.

Because the extremely high-velocity contrasts found for the LVZ of PS-9, it might prove interesting to perform a parameter study which includes one more level of structure complication by including layer dip. Figure 7 is the result of such a calcu-

lation. The bottom interfaces of PS-9 which include the LVZ were simply tilted toward the east preserving all layer thicknesses and velocities. A ray theoretical approach was used to calculate the response for this three-dimensional model and is described elsewhere (Langston, 1976c). Since all interfaces are parallel, the method, in this case, simply consists of assigning each ray an amplitude corresponding to a new incident angle and azimuth at the source and tracing it through the plane parallel model with a "local" ray parameter determined by the station azimuth and distance and structure dip. An eastward dipping model is shown because of the suggestions made by McKenzie and Julian (1971) and Lin (1974) for an eastward dipping slab.

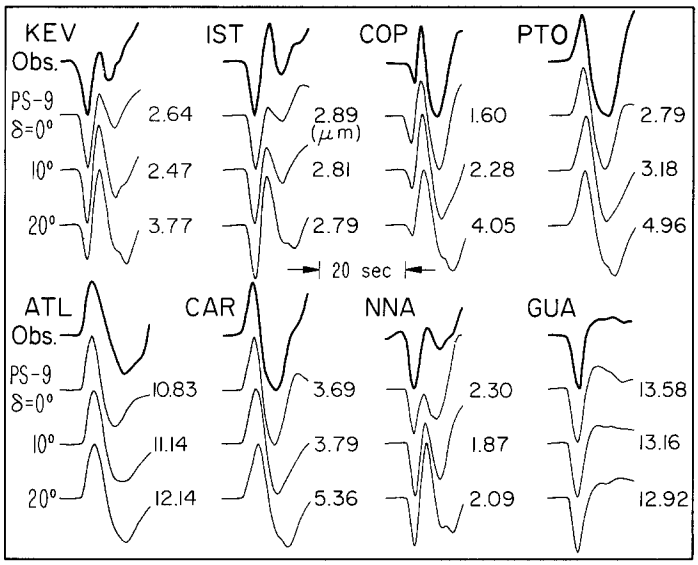

FIG. 7. Parameter study in which the horizontal layer interfaces at the LVZ of PS-9 are allowed to dip. At each station the *top trace* is the observed *P* wave and just below it is the synthetic for PS-9. Below this wave form are two synthetics for a 10°E and 20°E dipping LVZ.

Figure 7 shows the first 18 sec of eight representative *P* waves of Figure 2. The effect of layer dip manifests itself primarily in those very stations which were important in resolving the LVZ, e.g., KEV, IST, COP, and NNA. Stations in which direct *P* is predominant, such as ATL and GUA, show little change with increasing dip. The main effect of layer dip for all eastern azimuths is to have upgoing rays start from the focal sphere in a more easterly direction. Differences between the focal area azimuth and station azimuth can be up to 30°. This change in the relative amplitude between downgoing and upgoing rays due to the modified radiation pattern coupled with changes in the reflection coefficient for this particular source and structure model produces the effect of a direct tradeoff between layer dip (to the east) and LVZ interface contrasts. Although there is no way of knowing from these data whether planar dipping structure exists at Puget Sound it is very evident that it could have a very important effect on the particular velocity contrasts inferred from the horizontally layered model. A 50 per cent reduction could easily be possible, say for the $\delta = 20°$ case, but the general characteristics of the LVZ must still be included in the earth model.

Modeling the rotated *SH* waves revealed little about the source or structure. Figure 8 shows the six observed *SH* waves with corresponding synthetic seismograms

computed by ray techniques using the PS-9 model. Basically, the observed *SH* waves are very simple showing only the direct *S*. Most of the "glichiness" of these waves is due to digital noise in the rotation process. Since upgoing *S* is relatively small for these stations, none of the major discontinuities of PS-9 are directly observable except for the free surface. The phase *sS* is not readily apparent in the observations although it is theoretically small. Several possibilities can be presented. First, the *S*-velocity structure of PS-9 may be completely wrong so that *sS* time is significantly different. However, examination of the *SH* observations yields no consistent arrival at any other time. A second possibility is that local receiver crustal effects such as *S*-coupled *PL* waves may contaminate the tangential component. *S* waves are notorious for this and the position of *sS* relative to *S* makes this possibility very probable (Helmberger and Engen, 1974). A third and very likely possibility is that the earth model near the source is deficient. It could be that anelastic attenuation plays an important role. Some short-period results will be presented below which support this speculation.

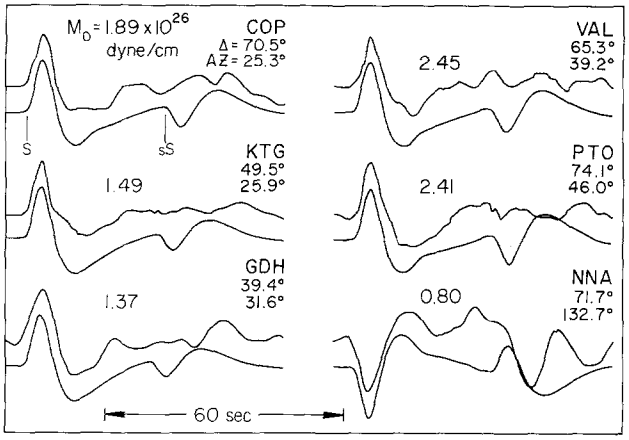

FIG. 8. Comparison of the observed and final synthetic *SH* waves. Same scheme as in Figure 2.

Scaling the synthetic direct *P* and *SH* waves to the long-period data yields a moment determination for the Puget Sound event. A value of $1.3 \pm 0.6 \times 10^{26}$ dyne-cm is obtained from 21 *P* waves (see Figure 3.2). The uncertainty given is the standard error. The six *SH* waves, Figure 8, yield an average value of $1.7 \pm 0.6 \times 10^{26}$ dyne-cm, slightly higher than the *P* waves but well within the uncertainties of the geometrical spreading correction and assumptions on attenuation. The average moment including both *P* and *S* waves, is $1.4 \pm 0.6 \times 10^{26}$ dyne-cm. The scatter in amplitudes, yet not in wave shape, can be considerable even for nearby stations. For example, compare IST and ATU, Figure 2.

An attempt was made to utilize the many short-period observations from this event to determine timing and amplitude information to help pin down the inferred structural discontinuities. Although the attempt eventually fell short of its original goals some interesting effects between the direct and reflected phases were observed.

An easy way to change a short-period record into a form suitable for stacking is to compute an envelope of the signal. Once the envelope is found for several records a suitable amplitude normalization is performed and the traces averaged with all seismograms lined up with respect to their first arrivals. A convenient way to compute the type of envelope needed here is to take the instantaneous amplitude of the

analytic signal (Farnbach, 1975). The analytic signal is defined by (Bracewell, 1965)

$$\begin{aligned} \hat{S}(t) &= f(t) - iF_{\mathrm{H}i}(t) \\ &= |\hat{S}(t)|\, e^{i\alpha(t)} \end{aligned} \tag{1}$$

where,

$f(t)$ = observed time series

$\hat{S}(t)$ = analytic signal

$F_{Hi}(t)$ = Hilbert transform of $f(t)$

$\alpha(t)$ = time varying phase

$|\hat{S}(t)|$ = instantaneous amplitude.

The Hilbert transform in equation (1) can simply be thought of as a convolution of $-1/\pi t$ with $f(t)$. Figure 9 shows an example of taking the instantaneous amplitude, $|\hat{S}(t)|$, of a short-period vertical P wave recorded at AFI. This method preserves the times and relative amplitudes of the arrivals and even makes the record a little easier to interpret visually. By no means does it purport to add any information; it simply makes it easier to work with the seismograms. The normalization was done by setting the area of the first 10 sec of the envelope to unity. This tended to boost the relative amplitude of sharp arrivals to that of emergent arrivals.

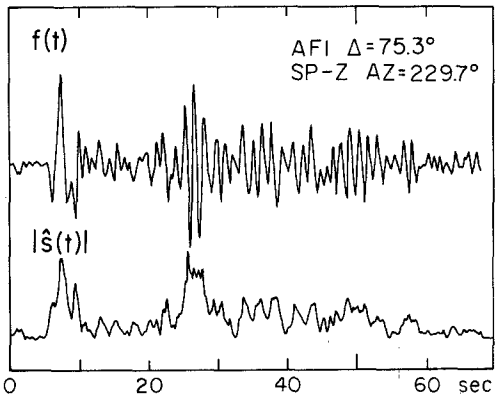

FIG. 9. Example of finding the envelope of a short-period record using the instantaneous amplitude of the analytic signal.

Figure 10 shows the results obtained from a stacking experiment. The traces labeled "P"are stacked envelopes of short-period vertical P waves grouped as a function of range. The range interval is indicated under each group name and the number in parentheses represents the number of seismograms used per group. Table 1 indicates the particular stations used in this grouping. The P-wave stacked traces show several interesting effects. In the first 10 sec two prominent arrivals are usually evident and are designated P and p_mP in the diagram. The first arrival is interpreted to be the direct P wave with p_mP being the reflection from the bottom of the LVZ. The timing agrees with the long-period result. This is not too useful except to show that the reflection has approximately the same frequency content as the direct wave.

This implies that the contrast at this boundary must be sharp, probably less than 2 km in transition. The most striking effect these traces demonstrate, however, is the very conspicuous absence of pP, especially at the smaller epicentral distances. A simple glance at the long-period wave forms in Figure 2 reveals that, except for the western stations, pP is at least as big as direct P and usually two or three times bigger. The relative amplitude of pP in groups a, b, and c of Figure 10 is at least half that of direct P. Not until stations with ranges greater than 75° are considered does pP start becoming apparent. This effect can be inferred to come from earth structure by using the information gleaned from p_mP. Because the frequency content of upgoing rays is similar to that of the downgoing rays, a source effect, such as directivity, can automatically be eliminated. All reflections should be apparent unless structure or attenuation effects cancel the arrivals.

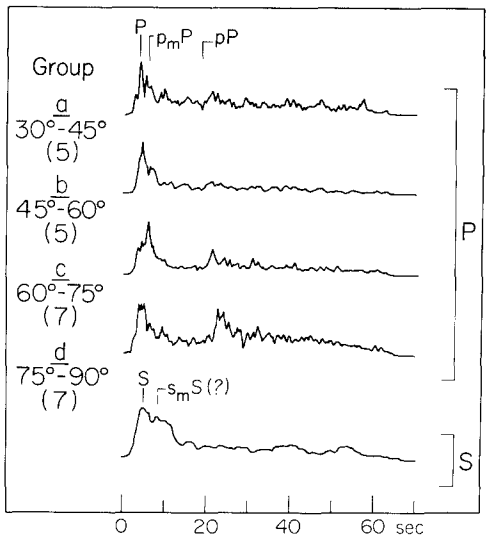

FIG. 10. Stacked envelopes of short-period P and S waves. The arrows point directly to the phase being identified except for the pP arrow, which designates the theoretical arrival time.

An explanation for this observation can be found in the geologic and structural framework of Puget Sound. Figure 11 is a map of southern Puget Sound with the epicenter plotted near the center (after Algermissen and Harding, 1965). The concentric circles are contours of the position pP hits the surface for a particular station distance. The hachured lines across Figure 11 represent a simplified version of structural discontinuities from the gravity and magnetic interpretation of Daneš *et al.* (1965). They are dashed where questionable. The tick marks are on the downthrown side of the inferred fault. The large numbers in parentheses are inferred depths to crystalline basement from the surface. This map readily demonstrates the great structural relief and complexity in the near-surface geology. The contours of pP are only approximate when considered from this approach since they were calculated using a plane-layered model, an assumption which clearly breaks down for the near-surface layers. Nevertheless, they should be useful to first order. Comparing the distance ranges and the structure gives a possible explanation for the amplitude behavior of short-period pP. For all stations at distances less than 75° pP bounces at points which have thick sections of sediment. For stations with ranges greater than that, pP bounces within the boundaries of the large horst or near its edge where sedi-

ment thicknesses are presumably smaller. This observation seems to correlate with the effects seen in the traces of Figure 10. Possibly, then, the attenuation of pP relative to P comes either from structurally disturbed sediments causing wave scattering or perhaps from anelastic attenuation. Either mechanism is feasible. An effective "Q" can be computed from these observations by using equation (2). A conservative estimate of the amplitude attenuation factor, a, is about $\frac{1}{3}$ for a 0.75-sec short-period sinusoid, and with a total travel time, T, of 17 sec gives

$$Q_{\text{eff}} = (-\omega T/2 \ln a) \tag{2}$$
$$= 65.$$

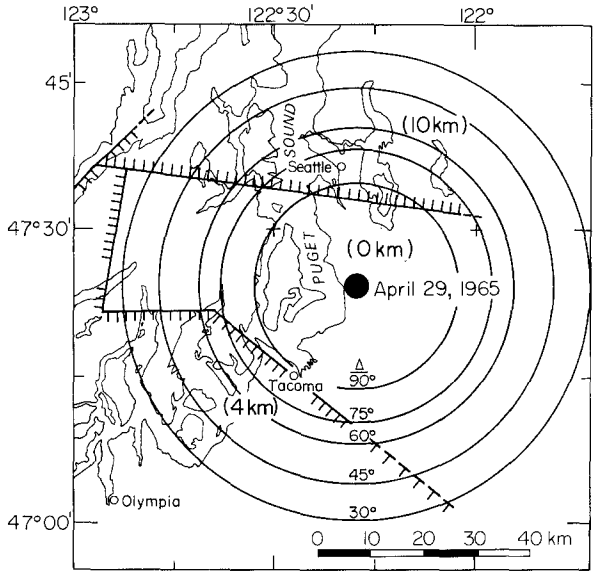

FIG. 11. Map of the southern Puget Sound area showing the epicenter for the 1965 event (after Algermissen and Harding, 1965). The concentric circles are contours of pP reflection points as a function of epicentral distance. The hachured lines are faults inferred by gravity and magnetics from Danes *et al.* (1965) with the tick marks on the downthrown side. The numbers in parenthesis are depth to basement in kilometers.

This amounts to convolving pP with another Q operator on top of the first (T/Q = 1.0) with a travel time to Q ratio of 0.3. This particular Q operator would have negligible effect on a long-period P wave form.

The realization that Puget Sound is structurally heterogeneous can explain why the shape details of pP are not fit by PS-9 for all azimuths (see Figure 2). In fact, it is surprising that the model works at all. Perhaps the pathological case of GDH, Figure 2, can have an explanation in this light.

Returning to Figure 10 one last point can be made using the short-period stacking procedure. The *bottom trace*, labeled "S," is the average of both horizontal short-period S-wave components at seven stations (Table 1). The result of the averaging revealed two arrivals roughly 3 sec apart. The first is interpreted to be direct S. Comparisons with each corresponding long-period component revealed that the short-period S started after any long-period $S - P$ precursors and correlation occurred where the long-period arrival was sharpest. The second arrival, because of its timing, is interpreted to be the reflection from the bottom of the LVZ. This arrival did not occur at all stations and there were significant wave-form variations between stations

to make this a tentative conclusion. It does give weak evidence against multiple source complications through the agreement in travel times for the inferred reflected *S* phase.

Discussion of the Earthquake Results

The source model presented here is an exceedingly simple one. The orientation agrees with previous studies and the time function is short and uncomplicated. It is certainly quite possible that there are other source complications but an earth model has been presented which, if anything, demonstrates the problems one has to deal with in order to discern these effects.

The earth model, on the other hand, is relatively complicated. In some respects it is heartening to see how some parts of the model agree with the geology and previous geophysics. For example, the inferred crustal thickness is about 15 km. Although crustal thickness is on the order of 30 km for central Puget Sound (Zuercher, 1975; Crosson, 1976), refraction results indicate a Conrad discontinuity at approximately this level and may be a possible interpretation for the observed transition. The low-velocity layers at the top of the model, needed to widen *pP* and attenuate *sP*, correlate nicely with the thick sections of presumably Tertiary sediments under the blanket of glacial till.

On the other hand, discovery of the massive LVZ in the uppermost mantle by these means presents many problems in uniqueness, although the model produces a good fit to all the *P* waves. Clearly, a check on this conclusion is desirable. One way to do this would be to examine another earthquake to see if the same structure effects are observable. The 1949 event would be the logical choice since it occurred nearby and at a depth of 70 km. The records, however, are not easily available and the orientation of the event, relative to the station coverage, might not be appropriate for observing these effects. Because the inferred structural boundaries of the LVZ are so distinct they should be directly observable from upcoming phase conversions and reverberations using teleseismic sources for stations situated over the structure. Fortunately, there are several long-period WWSS and Canadian network stations nearby to test the model. The WWSSN station at Corvallis, Oregon, was studied in this manner (Langston, 1977b) and although the details of the earth model are different from PS-9, the distinct LVZ was again found.

Note that a classical interpretation of where the moho occurs was not made here. An interface between the LVZ and "crustal" section may exist but was not resolved by the data. The possibility exists that the moho may certainly be above the LVZ or it may form the lower boundary of the LVZ, depending on the velocity values assigned to the model and other complications such as dipping or discontinuous structure. The plane layered model presented here is clearly only a crude approximation to the effects which have distorted the body waves from the Puget Sound earthquake.

Conclusions

A major, distinct low-velocity zone is inferred in the uppermost mantle under Puget Sound by modeling reflected arrivals in the long-period *P*-wave forms from the 1965 Puget Sound earthquake. The LVZ occurs in the depth interval of 41 to 56 km and is sandwiched between layers having mantle velocities. The velocity contrast at the bottom interface of the LVZ must be on the order of 2.5 km/sec as inferred from the theoretical relative *P* amplitudes from the point dislocation source, assuming horizontal structure. If eastward dipping structure is allowed, the velocity contrasts in the LVZ trade-off directly with dip.

The crust of southern Puget Sound has a thick sediment section near the surface as inferred from the shapes of the *pP* and *sP* phases. This is consistent with other geophysical studies.

The earthquake source parameters determined by the *P*- and *SH*-wave-form study are the following: 70° dip to the east; 344° strike; −75° rake, making it a normal dip-slip fault, consistent with previous studies; seismic moment of $1.4 \pm 0.6 \times 10^{25}$ dyne-cm; 63 km depth; and a simple time history represented by a triangular far-field source function with a rise time of 0.5 sec and a falloff of 2.5 sec. The depth is constrained by *pP* and *sP* travel times.

The synthetic *P*- and *SH*-wave forms computed from the given source and earth models reproduce the major azimuthal variations which occur in the data wave forms.

A short-period stacking procedure utilizing the instantaneous amplitude of the analytic signal is presented and used to find reflected arrivals. An apparent attenuation is found for short-period versus long-period *pP* and is correlated with sediment thickness at the reflection point. The amplitude discrepancy yields an effective Q of about 65 for the earth structure above the earthquake.

Acknowledgments

This research was supported by the Advanced Research Projects Agency of the Department of Defense and was monitored by the Air Force Office of Scientific Research under Contract F44620-72-C-0078 and by the National Science Foundation Grant EAR 76-06619.

References

Algermissen, S. T. and S. T. Harding (1965). Preliminary Seismological Report, in *The Puget Sound, Washington Earthquake of April 29*, 1965, U.S. Department of Commerce, Coast and Geodetic Survey, U.S. Government Printing Office, Washington, 51 pages.

Atwater, T. (1970). Implications of plate tectonics for the Cenozoic tectonic evolution of Western North America, *Bull. Geol. Soc. Am.* **81**, 3513–3536.

Berg, J. W., L. T. Trembly, D. A. Emilla, J. R. Hutt, J. M. King, L. T. Long, W. R. McKnight, S. K. Sarmah, R. Souders, J. V. Thiruvathukal, D. A. Vossler (1966). Crustal refraction profile, Oregon Coast Range, *Bull. Seism. Soc. Am.* **56**, 1357–1362.

Bracewell, R. (1965). *The Fourier Transform and Its Applications*, McGraw-Hill, New York, 381 pages.

Bromery, R. W. and P. D. Snavely, Jr. (1964). Geologic interpretation of reconnaissance gravity and aeromagnetic surveys in northwestern Oregon, *U.S. Geol. Surv., Bull. 1181-N*.

Chandra, U. (1974). Seismicity, earthquake mechanisms, and tectonics along the western coast of North America, from 42°N to 61°N, *Bull. Seism. Soc. Am.* **64**, 1529–1549.

Crosson, R. S. (1972). Small earthquakes, structure, and tectonics of the Puget Sound Region, *Bull. Seism. Soc. Am.* **62**, 1133–1171.

Crosson, R. S. (1976). Crustal structure modeling of earthquake data, 2. Velocity structure of the Puget Sound Region, Washington, *J. Geophys. Res.* **81**, 3047–3054.

Daneš, Z. F. (1969). Gravity results in western Washington, *EOS*, **50**, 348–350.

Daneš, Z. F., M. M. Bonno, E. Brau, W. D. Gilham, T. F. Hoffman, D. Johnson, M. H. Jones, B. Malfait, J. Masten, and G. O. Teague (1965). Geophysical investigation of the southern Puget Sound area, Washington, *J. Geophys. Res.* **70**, 5573–5580.

Dehlinger, P., E. F. Chiburis, and M. M. Collver (1965). Local travel-time curves and their geologic implications for the Pacific Northwest States, *Bull. Seism. Soc. Am.* **55**, 587–607.

Dickinson, W. R. (1970). Relations of andesites, granites, and derivative sandstones to arc-trench tectonics, *Rev. Geophys., Space Phys.* **8**, 813–860.

Farnbach, J. S. (1975). The complex envelope in seismic signal analysis, *Bull. Seism. Soc. Am.* **65**, 951–962.

Fuchs, K. (1966). The transfer function for *P* waves for a system consisting of a point source in a layered medium, *Bull. Seism. Soc. Am.* **56**, 75–108.

Hagiwara, T. (1958). A note on the theory of the electromagnetic seismograph, *Bull. Res. Inst., Tokyo Univ.*, **36**, 139–164.

Hamilton, W. and W. B. Myers (1966). Cenozoic tectonics of the Western United States, *Rev. Geophys. and Space Physics* **4**, 509–549.

Harkrider, D. G. (1964). Surface waves in multilayered elastic media, I. Rayleigh and Love waves from buried sources in a multilayered elastic half-space, *Bull. Seism. Soc. Am.* **54,** 627–679.

Haskell, N. A. (1953). The dispersion of surface waves on multilayered media, *Bull. Seism. Soc. Am.* **43,** 17–34.

Helmberger, D. V. and G. R. Engen (1974). Upper mantle shear structure, *J. Geophys. Res.* **79,** 4017–4028.

Isacks, B. and P. Molnar (1971). Distribution of stresses in the descending lithosphere from a global survey of focal-mechanism solutions of mantle earthquakes, *Rev. Geophys. Space Phys.* **9,** 103–174.

Langston, C. A. (1976a). A body wave inversion of the Koyna, India, earthquake of 10 December 1967 and some implications for body wave focal mechanisms, *J. Geophys. Res.* **81,** 2517–2529.

Langston, C. A. (1977b). Corvallis, Oregon, Crustal and upper mantle receiver structure from teleseismic *P* and *S* waves, *Bull. Seism. Soc. Am.* **67,** 713–724.

Langston, C. A. (1977c). The effects of planar dipping structure on source and receiver responses for constant ray parameter **67,** (in press).

Langston, C. A. and D. V. Helmberger (1975). A procedure for modeling shallow dislocation sources, *Geophys. J.* **42,** 117–130.

Lin, J. W. (1974). A study of upper mantle structure in the Pacific Northwest using *P* waves from teleseisms, *Ph.D. Thesis,* University of Washington, 98 pp.

McCollom, R. L. and R. S. Crosson (1975). An array study of upper mantle velocity in Washington state, *Bull. Seism. Soc. Am.* **65,** 467–482.

McKenzie, D. and B. Julian (1971). Puget Sound, Washington, earthquake and the mantle structure beneath the northwestern United States, *Geol. Soc. Am. Bull.* **82,** 3519–3524.

Nuttli, O. W. (1952). The western Washington earthquake of April 13, 1949, *Bull. Seism. Soc. Am.* **42,** 21–28.

Press, F. (1966). Seismic velocities, in *Handbook of Physical Constants, Geol. Soc. Am. Mem. 97.*

Raff, A. D. and R. G. Mason (1961). Magnetic survey off the west coast of North America, 40°N latitude to 52°N latitude, *Bull. Geol. Soc. Am.* **72,** 1267–1270.

Silver, E. A. (1971a). Transitional tectonics and late Cenozoic structure of the continental margin off northernmost California, *Bull. Geol. Soc. Am.* **82,** 1–22.

Silver, E. A. (1971b). Small plate tectonics in the northeastern Pacific, *Bull. Geol. Soc. Am.* **82,** 3491–3496.

Silver, E. A. (1972). Pleistocene tectonic accretion of the continental slope of Washington, *Marine Geol.* **13,** 239–249.

Snavely, P. D. and H. C. Wagner (1963). Tertiary geologic history of western Oregon and Washington, *Div. Mines Geol. Report of Invest. 22,* 25 pages.

Snavely, P. D., N. S. MacLeod, H. C. Wagner (1968). Tholeiitic and alkalic basalts of the Eocene Siletz River volcanics, Oregon Coast Range, *Am. J. Sci.* **266,** 454–481.

Tatel, H. E. and M. A. Tuve (1955). Seismic exploration of a continental crust, *Geol. Soc. Am. Spec. Paper 62,* 35–50.

Tobin, D. G. and L. R. Sykes (1968). Seismicity and tectonics of the northeast Pacific Ocean, *J. Geophys. Res.* **73,** 3821–3845.

Vine, F. J. (1966). Spreading of the ocean floor: New evidence, *Science* **154,** 1405–1414.

Vine, F. J. and J. T. Wilson (1965). Magnetic anomalies over a young oceanic ridge off Vancouver Island, *Science* **150,** 485–489.

White, W. R. H. and J. C. Savage (1965). A seismic refraction and gravity study of the Earth's crust in British Columbia, *Bull. Seism. Soc. Am.* **55,** 463–486.

Wilson, J. T. (1965). Transform faults, oceanic ridges and magnetic anomalies southwest of Vancouver Island, *Science* **150,** 482–485.

Zuercher, H. (1975). A study of the crust in Puget Sound using a fixed seismic source, *M. S. Thesis,* University of Washington, 62 pages.

Seismological Laboratory
Division of Geological and Planetary Sciences
California Institute of Technology
Pasadena, California 91125
Contribution No. 2822.

Manuscript received September 23, 1976